Physica C 507 (2014) 70–74

Contents lists available at ScienceDirect

Physica C

journal homepage: www.elsevier.com/locate/physc

Preparation and characterisation of Os doped MgB_2

J.-C. Grivel *, S. Namazkar, A. Alexiou, O.J. Holte

Department of Energy Conversion and Storage, Technical University of Denmark, 4000 Roskilde, Denmark

ARTICLE INFO

Article history:
Received 8 August 2014
Received in revised form 10 October 2014
Accepted 19 October 2014
Available online 28 October 2014

Keywords:
MgB_2
Doping
Osmium

ABSTRACT

Polycrystalline samples with $Mg_{1-x}Os_xB_{2.04}$ nominal stoichiometry were made by reacting elemental powders at 800 °C under argon atmosphere. Based on XRD diffraction patterns, EDS analysis and magnetisation measurements, it is found that Os can replace up to about 1 at.% Mg in the MgB_2 lattice. Beyond this doping level, unreacted Os and Mg-rich Mg–Os impurity phases are formed. The *a*-axis parameter contracts upon doping while the superconducting transition temperature decreases at a rate of 2.1 K/at.% Os substitution. At 10 K, Os doping induces an improvement of the normalised critical current density under applied magnetic fields in excess of 0.5 T, indicating a modest enhancement of flux pinning in this range.

1. Introduction

Owing to its relatively high critical temperature ($T_c \approx 40$ K), relative abundance of its constituent elements and low activity under neutron irradiation [1,2], MgB_2 is foreseen as a strong candidate for many large scale applications such as coils in cryogen free MRI-systems [3,4], induction heating devices [5] and other applications as diverse as fault-current limiters, generators, transformers, magnetic shields for manned deep-space missions, etc. [6,7]. However, the critical current densities achievable in MgB_2 wires under magnetic fields need to be enhanced for enabling the realisation of most of the above applications. In order to improve the performance of MgB_2 in high magnetic fields, two strategies are commonly used: introducing nanometer-sized impurities as artificial flux pinning centres or doping with foreign elements. In view of the latter, carbon, which can replace up to about 30 at.% B in the MgB_2 lattice, is remarkably efficient but further improvements are still desirable [8–11]. For this reason, research activities are ongoing to find other potential options for enhancing the flux pinning strength of MgB_2 like for example dual doping on both B and Mg sites. Except for the case of Al that can be substituted for Mg up to at least 40% [12–15], doping on the Mg sites is usually limited to few atomic percent or even less [16–33]. Among the transition metal elements, only few results have been published on the possibility of substituting platinum group metal elements in MgB_2. Besides Pt, which was studied in association with SiC doping [34], only Ir and Ru appear to have been reported to have a limited but measurable solubility and result in a decrease of T_c [28,32]. The present contribution reports on the possible substitution of Os for Mg in MgB_2 and its effects on structure and T_c.

2. Experimental details

Mg (Alfa Aesar, 99.8% purity), amorphous boron (Aldrich, 95–97%) and Os (Alfa Aesar, 99.8%) were used as starting reagents. The elemental powders were mixed in $Mg_{1-x}Os_xB_{2.04}$ ($0.000 \leqslant x \leqslant 0.040$, $\Delta x = 0.005$) nominal ratios and homogenised by manual grinding in an agate mortar. The choice of a small B excess in the nominal compositions is based on a previous study showing that for this specific grade of amorphous boron powder, which contains a slight amount of Mg as impurity, the best results in terms of phase purity were obtained for this particular composition in undoped MgB_2 [35]. After grinding, the powders were pressed into pellets (1 g powder, 12 mm diameter under a pressure of 1.8 kbar). The pellets were wrapped into Ti foils of 32 μm thickness that act as oxygen getter and reduce the risk of Mg losses during heat treatment. After a first sintering at 700 °C for 1 h, the samples were sintered twice during 1 h at 800 °C with intermediate grinding and repressing. All heat treatments were performed under Ar atmosphere.

XRD patterns were recorded in a STOE X-ray diffractometer with Cu Kα radiation ($\lambda = 1.5406$ Å) on powdered samples after the final treatment at 800 °C. Silicon powder was mixed to the samples after grinding as an internal standard for lattice parameters calculations using the UnitCell least square refinement programme [36]. The microstructure of the samples and the composition of the various phases present after sintering at 800 °C were studied by means of scanning electron microscopy

* Corresponding author. Tel.: +45 4677 4739; fax: +45 4677 5758.
E-mail address: jean@dtu.dk (J.-C. Grivel).

http://dx.doi.org/10.1016/j.physc.2014.10.010
0921-4534/

(SEM) in a table-top TM3000 microscope from HITACHI equipped with a QUANTAX 70 EDS analyser. The critical temperature (T_c) was determined as the onset of the diamagnetic transition from the real component of ac-susceptibility measurements performed between 5 K and 45 K with an applied magnetic field of 0.1 mT rms and 17 Hz frequency in a CRYOGENIC Ltd Mini-CFMS. A vibrating sample magnetometry (VSM) setup was used in the same instrument to record M(B) loops at 10 K and 30 K on powders loaded in sample holders with 4.5 mm internal diameter.

3. Results and discussion

The XRD patterns of all samples after the second sintering treatment at 800 °C are presented in Fig. 1. The Os-free sample contains a minor amount of MgO but consists otherwise of MgB_2 only. Increasing the nominal Os content results in the appearance of new reflections, with elemental Os clearly visible from $x = 0.025$ and peaks from an unidentified phase emerging from the background around $x = 0.015$. The lattice parameters of the MgB_2 phase are plotted in Fig. 2 and listed in Table 1. The *a*-axis parameter sharply decreases up to $0.015 < x < 0.020$ before becoming constant within the standard deviation limits. In contrast, the *c*-axis parameter is not clearly affected by Os doping. It seems to follow a trend for decreasing values, but this continues up to the maximum doping level ($x = 0.040$). The ion radius of Os^{4+} is significantly lower than that of Mg^{2+} (63 pm versus 72 pm in VI-fold coordination [37]) and this could explain the decrease of the *a*-axis lattice parameter up to a maximum solubility of about $x = 0.015$. As for the slight decrease of the *c*-axis parameter beyond $x = 0.015$, it could be an indirect consequence of the formation of an impurity phase containing Mg and/or B in an atomic ratio different from MgB_2, possibly in association with Os, because this would lead to a change of the stoichiometry of the remaining MgB_2 matrix and it has been previously shown that modifications of the Mg:B ratio in MgB_2 results in subtle changes of the lattice parameters [38–42].

The critical temperature (Fig. 3) decreases rapidly up to $x = 0.010$ and seems to become almost constant beyond $x = 0.012$ approximately, as estimated by extrapolating the initial slope and the T_c values for the highest doping levels. The onset of the diamagnetic transition, down to 50% of the complete transition is also shown in Fig. 3. It appears that the transition is sharp but tends to broaden beyond the solubility limit. The apparent slow decrease of T_c for $x > 0.010$ can be explained in a similar way as for the decrease of the *c*-axis parameter discussed above. By comparison

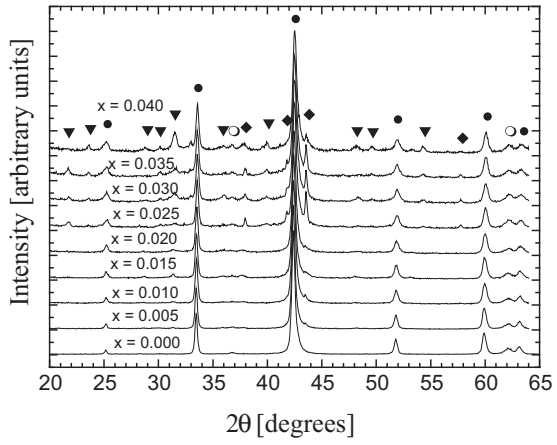

Fig. 1. X-ray diffraction patterns of the samples with $Mg_{1-x}Os_xB_{2.04}$ nominal composition after sintering twice at 800 °C for 1 h in Ar. ●: MgB_2; ○: MgO; ♦: Os; ▼: unidentified phase.

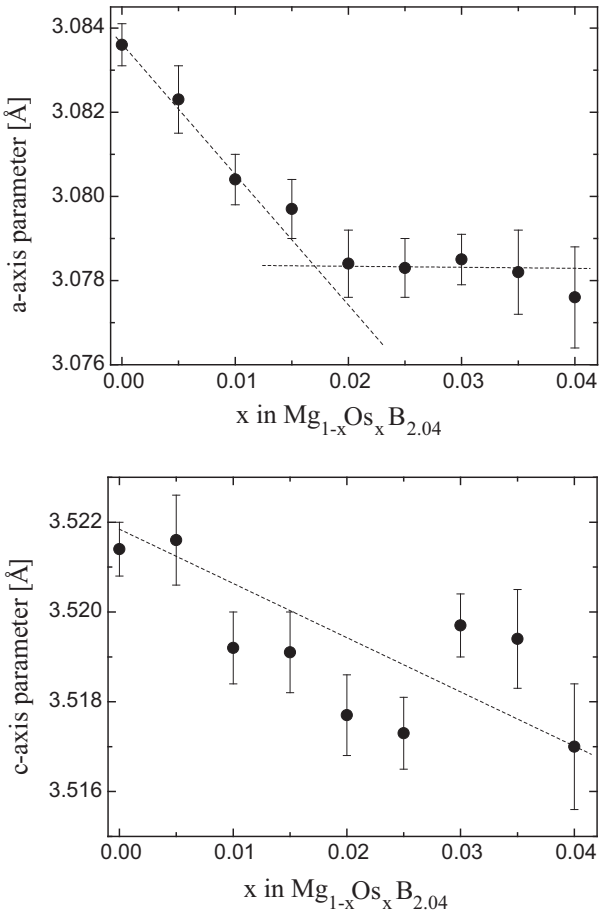

Fig. 2. Unit cell parameters of MgB_2 as a function of nominal composition. Dashed lines are guides to the eye.

Table 1
a-Axis and *c*-axis parameters as well as critical temperature (T_c) of the $Mg_{1-x}Os_xB_{2.04}$ samples.

x in $Mg_{1-x}Os_xB_{2.04}$	*a*-Axis (Å)	*c*-Axis (Å)	T_c (K)
0.000	3.0836(5)	3.5214(6)	38.9(3)
0.005	3.0823(8)	3.5216(10)	37.9(3)
0.010	3.0804(6)	3.5192(8)	36.8(3)
0.015	3.0797(7)	3.5191(9)	36.9(3)
0.020	3.0784(8)	3.5177(9)	36.4(3)
0.025	3.0783(7)	3.5173(8)	36.5(3)
0.030	3.0785(6)	3.5197(7)	36.1(3)
0.035	3.0782(10)	3.5194(11)	35.9(3)
0.040	3.0776(12)	3.5170(14)	36.1(3)

with the lattice parameter evolution and the XRD patterns, it can be concluded that the solubility limit of Os in MgB_2 is situated between $x = 0.010$ and $x = 0.015$. This is further confirmed by EDS measurements performed on a polished cross-section of the sample with $Mg_{0.96}Os_{0.04}B_{2.04}$ nominal stoichiometry, which yield an average Mg:Os atomic ratio of 98.96:1.04 with a standard deviation $\sigma = 0.38$ for a total of 20 local analyses performed on areas corresponding to MgB_2 grains that do not show evidence for secondary phase particles precipitates down to a scale of 0.5 μm. As evidenced in Fig. 4, which shows the EDS mapping of a $80 \times 60\ \mu m^2$ area of the $Mg_{0.96}Os_{0.04}B_{2.04}$ sample after sintering twice at 800 °C, Os-rich particles with relatively large diameters (up to 12 μm) are present within the "MgB_2" matrix. EDS quantification suggests in a first instance that these particles consist of a Mg–Os intermetallic alloy containing between 13 and 36 at.% Os.